

Quantitative comparison between Type Ia supernova spectra at low and high redshifts: A case study

G. Garavini^{1,4}, G. Folatelli², S. Nobili¹, G. Aldering³, R. Amanullah¹, P. Antilogus⁴, P. Astier⁴, G. Blanc⁵, J. Bronder⁶, M. S. Burns⁷, A. Conley^{3,8}, S. E. Deustua⁹, M. Doi¹⁰, S. Fabbro¹¹, V. Fadeyev³, R. Gibbons¹², G. Goldhaber^{3,8}, A. Goobar¹, D. E. Groom³, I. Hook⁶, D. A. Howell¹³, N. Kashikawa¹⁴, A. G. Kim³, M. Kowalski³, N. Kuznetsova³, B. C. Lee³, C. Lidman¹⁵, J. Mendez^{16,17}, T. Morokuma¹⁰, K. Motohara¹⁰, P. E. Nugent³, R. Pain⁴, S. Perlmutter^{3,8}, R. Quimby³, J. Raux⁴, N. Regnault⁴, P. Ruiz-Lapuente¹⁷, G. Sainton⁴, K. Schahmanche⁴, E. Smith¹², A. L. Spadafora³, V. Stanishev¹, R. C. Thomas³, N. A. Walton¹⁸, L. Wang³, W. M. Wood-Vasey^{3,8}, and N. Yasuda¹⁹

(The Supernova Cosmology Project)

¹ Department of Physics, Stockholm University, Albanova University Center, S-106 91 Stockholm, Sweden

² Observatories of the Carnegie Institution of Washington, 813 Santa Barbara St., Pasadena, CA 91101

³ E. O. Lawrence Berkeley National Laboratory, 1 Cyclotron Rd., Berkeley, CA 94720, USA

⁴ LPNHE, CNRS-IN2P3, University of Paris VI & VII, Paris, France

⁵ Osservatorio Astronomico di Padova, INAF, vicolo dell'Osservatorio 5, 35122 Padova, Italy

⁶ Department of Physics, University of Oxford, Nuclear & Astrophysics Laboratory, Keble Road, Oxford, OX1 3RH, UK

⁷ Colorado College, 14 East Cache La Poudre St., Colorado Springs, CO 80903

⁸ Department of Physics, University of California Berkeley, Berkeley, 94720-7300 CA, USA

⁹ American Astronomical Society, 2000 Florida Ave, NW, Suite 400, Washington, DC, 20009 USA.

¹⁰ Institute of Astronomy, School of Science, University of Tokyo, Mitaka, Tokyo, 181-0015, Japan

¹¹ CENTRA e Dep. de Fisica, IST, Univ. Tecnica de Lisboa

¹² Department of Physics and Astronomy, Vanderbilt University, Nashville, TN 37240, USA

¹³ Department of Astronomy and Astrophysics, University of Toronto, 60 St. George St., Toronto, Ontario M5S 3H8, Canada

¹⁴ National Astronomical Observatory, Mitaka, Tokyo 181-0058, Japan

¹⁵ European Southern Observatory, Alonso de Cordova 3107, Vitacura, Casilla 19001, Santiago 19, Chile

¹⁶ Isaac Newton Group, Apartado de Correos 321, 38780 Santa Cruz de La Palma, Islas Canarias, Spain

¹⁷ Department of Astronomy, University of Barcelona, Barcelona, Spain

¹⁸ Institute of Astronomy, Madingley Road, Cambridge CB3 0HA, UK

¹⁹ Institute for Cosmic Ray Research, University of Tokyo, Kashiwa, 277 8582 Japan

Abstract. We develop a method to measure the strength of the absorption features in Type Ia supernova (SN Ia) spectra and use it to make a quantitative comparison between the spectra of Type Ia supernovae at low and high redshifts. In this case study, we apply the method to 12 high-redshift ($0.212 \leq z \leq 0.912$) SNe Ia observed by the Supernova Cosmology Project. Through measurements of the strengths of these features and of the blueshift of the absorption minimum in Ca II H&K, we show that the spectra of the high-redshift SNe Ia are quantitatively similar to spectra of nearby SNe Ia ($z < 0.15$). One supernova in our high redshift sample, SN 2002fd at $z=0.279$, is found to have spectral characteristics that are associated with peculiar SN 1991T/SN 1999aa-like supernovae.

1. Introduction

Type Ia supernovae (SNe Ia) are excellent distance indicators and have been used to show that the expansion of the Universe is currently accelerating (Perlmutter et al. 1998; Garnavich et al. 1998; Schmidt et al. 1998;

Riess et al. 1998; Perlmutter et al. 1999; Knop et al. 2003; Tonry et al. 2003; Barris et al. 2004; Riess et al. 2004; Krisciunas et al. 2005; Astier et al. 2006; Wood-Vasey et al. 2007).

Recently, both the SNLS¹ and ESSENCE² projects, which aim to use hundreds of SNe Ia to constrain the nature of dark energy through the measurement of the equation-of-state parameter, have reported their first results. The control of the systematic uncertainties is critical to their success. Among the possible systematic effects, evolution of the SNe Ia population over cosmological time-scales is one of the most important and least understood.

Spectra of SNe Ia are well-suited to study potential evolutionary effects. For example, the average metallicity of the Universe increases with cosmic time, so it is reasonable to expect that high-redshift SNe Ia are in environments that have lower average metallicity than those of nearby SNe Ia. The effect on the spectral energy distribution of a lower metallicity progenitor has been modeled by Hoefflich et al. (1998) and Lentz et al. (2000). These studies find that such SNe Ia, especially at early epochs, are expected to show enhanced flux in the UV, weaker absorption features in the optical and a shift in the absorption minima of optical features to longer wavelengths.

With the large number of well-observed low-redshift supernovae now available, a wide range of spectral diversity is being found (Branch et al. (2006, see e.g.)). The physical origin of these differences is still not completely understood making it difficult to predict their possible evolution with redshift. Statistical studies are useful to probe differences between high and low-redshift SN Ia data sets. So far, few distant SN Ia spectra have been compared with low-redshift data sets in a quantitative manner (Perlmutter et al. 1998; Coil et al. 2000; Barris et al. 2004; Riess et al. 2003; Blakeslee et al. 2003; Matheson et al. 2005; Hook et al. 2005; Balland et al. 2006; Howell et al. 2005; Blondin et al. 2006), and few spectroscopically confirmed high-redshift SNe Ia have been reported as peculiar (two SN 1991T/SN 1999aa-like SNe Ia in Matheson et al. (2005); one, as we will see, in the present paper). Hereafter, we follow the convention of describing SN 1991T/SN 1999aa-like SNe Ia by using "91T-like" to represent both SN Ia subtypes.

During 2000, 2001 and 2002, the Supernova Cosmology Project (SCP) obtained spectra of 20 high-redshift SNe Ia with FORS2 on the ESO Very Large Telescope (Lidman et al. 2005). In this paper, we analyze the 14 spectra of 12 SN Ia with the highest signal-to-noise ratios and perform a quantitative comparison between these spectra and the spectra of low-redshift SNe Ia. The definition of a newly introduced spectral indicator for Type Ia supernovae, namely pseudo-equivalent width, is given in section 2. The data-sets we apply the method to are presented in section 3. The properties of the pseudo-equivalent width for SNe Ia are given in section 4 together with the result of the comparison between high- and low-redshift SNe Ia. Summary and conclusions are given in section 5.

2. Method

We use two spectral indicators to compare high- and low-redshift SN Ia spectra:

- 1) the wavelength of the absorption minimum at $\sim 3750 \text{ \AA}$, which is largely due to Ca II H&K, and
- 2) newly-introduced pseudo-EW measurements of features associated with Ca II H&K, Mg II and Fe II.

2.1. Pseudo-Equivalent Widths of SNe Ia

The spectra of Type Ia supernovae are very characteristic and, in comparison with supernovae of other types, relatively homogeneous. Spectral features are broad, reflecting the high velocities of the ejecta ($\sim 10000 \text{ km s}^{-1}$), and evolve with phase. However, differences between different Type Ia supernovae have been noted (see Filippenko (1997) for a review). In some cases the differences are dramatic and have resulted in the definition of SNe Ia subtypes.

The pseudo-equivalent width (pseudo-EW), first described in Folatelli (2004), can be used as a spectral indicator. It is described in detail in the following section.

2.2. Definition

The equivalent width, as used in stellar spectroscopy, can be used to measure the strength of absorption features in supernova spectra. However, the relationship between this quantity and the physical properties of the SN Ia ejecta is complex. In a SN Ia spectrum the overlap of thousands of lines give rise to a "pseudo" continuum thus a real continuum can not be identified. Because of this distinction with the definition of equivalent widths we use the term "pseudo-equivalent widths" to refer to our measurements. This does not prevent us from using this well-defined quantity, nor does it not allow us from building a consistent set of measurements for all SNe Ia in our data-sets.

In this analysis, we define an absorption feature as a wavelength region that is bounded by two local flux maxima. Fig. 1 shows eight such regions, corresponding to the eight strongest absorption features at optical wavelengths in supernova spectra up to approximately one month after maximum light. Each feature is marked with a number from 1 to 8 and each number corresponds to a mnemonic name. The upper and lower limits of the features vary in time (because of the SN Ia envelope expansion), and from SN Ia to SN Ia at a given phase (i.e. SN Ia spectral diversity). We give ranges for these limits in Table 1.

As already mentioned, in order to measure a pseudo-EW, a pseudo-continuum must be determined. We define the pseudo-continuum as the straight line fit through the two local maxima that bound a feature³ (see panel (b) in Fig. 1). A detailed explanation of the measurement technique is given in section 2.3.

¹ <http://www.cfht.hawaii.edu/SNLS/>

² <http://www.ctio.noao.edu/essence/>

³ The chosen maxima are those that maximize the wavelength span of the feature with the restriction that the derived pseudo-continuum does not intersect the spectrum within the

Once the pseudo-continuum is defined, the pseudo-EW is computed for each feature within its wavelength limits. The spectrum is divided by the pseudo-continuum and the resulting area of the feature is measured (in units of \AA). In this case, the calculation was approximated by a simple rectangular integration method:

$$\text{pseudo-EW} = \sum_{i=1}^N \left(1 - \frac{f_{\lambda}(\lambda_i)}{f_c(\lambda_i)} \right) \Delta\lambda_i, \quad (1)$$

where λ_i ($i = 1, \dots, N$) are the central wavelengths of the bins of size $\Delta\lambda_i$, $f_{\lambda}(\lambda_i)$ is the measured flux in bin i , and $f_c(\lambda_i)$ is the fitted pseudo-continuum flux evaluated at the same points. Deviating points due to bad pixels, night sky residuals, or narrow host-galaxy lines were rejected using a 3σ -clipping algorithm.

Table 1 Feature limits.

Feature ID	Mnemonic Label	Blue-ward limit range (\AA)	Red-ward limit range (\AA)
1	“Ca II H&K”	3500 – 3800	3900 – 4100
2	“Si II 4000”	3900 – 4000	4000 – 4150
3	“Mg II 4300”	3900 – 4150	4450 – 4700
4	“Fe II 4800”	4500 – 4700	5050 – 5550
5	“S II W”	5150 – 5300	5500 – 5700
6	“Si II 5800”	5550 – 5700	5800 – 6000
7	“Si II 6150”	5800 – 6000	6200 – 6600
8	“Ca II IR”	7500 – 8000	8200 – 8900

The 1σ statistical uncertainty was computed by error propagation from the estimated uncertainties in the spectral flux (σ_f) and in the pseudo-continuum (σ_c):

$$\sigma_{\text{pseudo-EW}} = \left[\sum_{i=1}^N \left(\frac{\sigma_{f_i}^2(\lambda_i)}{f_c^2(\lambda_i)} + \frac{f_{\lambda}^2(\lambda_i)}{f_c^4(\lambda_i)} \sigma_{c_i}^2(\lambda_i) \right) (\Delta\lambda_i)^2 \right]^{1/2}. \quad (2)$$

By definition, the rest-frame pseudo-equivalent width is redshift independent and thus provides a useful tool for comparing spectra from different objects over a wide range of redshifts.

2.3. Measurement technique

Measuring pseudo-equivalent widths on high signal-to-noise ratio spectra is relatively simple since the local maxima bounding an absorption feature can be identified easily. On low signal-to-noise data the measurements are more difficult. For comparing high redshift supernovae (which generally have low signal-to-noise) with local SN Ia spectra, we have established a measurement technique (to be applied on spectra regardless of their signal-to-noise ratio) that minimizes possible systematic effects.

To measure the pseudo-EW of a spectral feature the local pseudo-continuum must be determined. To perform this operation we proceeded as follows:

feature limits with the possible exception of noise artifacts in case of low signal-to-noise ratio data.

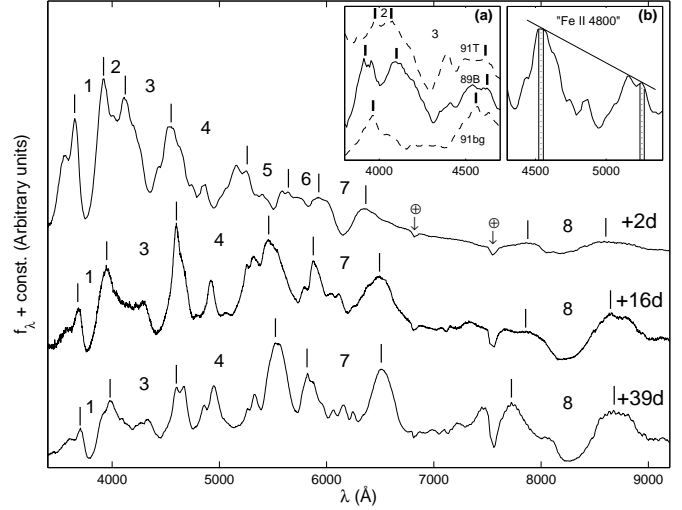


Fig. 1 SNe Ia spectral evolution and feature definitions for three epochs: 2, 16 and 39 days after maximum light. Numerical labels correspond to the following adopted feature names: 1- “Ca II H&K”; 2- “Si II 4000”; 3- “Mg II 4300”; 4- “Fe II 4800”; 5- “S II W”; 6- “Si II 5800”; 7- “Si II 6150”; and 8- “Ca II IR”. Short vertical lines show the approximate positions where the pseudo-continuum is taken in each case. Feature ranges change with time and, due to blending, some weaker features are not considered at later epochs. Note that after 2-3 weeks past maximum light, the selected pseudo-continuum points correspond to emission peaks. *Panel (a)*: the region around features #2 and #3 for near-maximum spectra of SN 1991T (top), SN 1989B (middle), and SN 1991bg (bottom). Feature #2 is not defined in the case of 1991bg-like SNe Ia because the region is dominated by absorption from Ti II. Adopted feature limits are marked with vertical lines. *Panel (b)*: an example of the pseudo-continuum trace for “Fe II 4800” on a normal SN Ia near the time of maximum light. Here, solid vertical lines show the regions where the pseudo-continuum is fitted. Dotted lines mark the bounds used to measure the pseudo-EW.

- The two local maxima that bound the absorption feature are visually identified and marked. These are the bounds used in performing the sum in Eqn. 1.
- A small wavelength region (to which hereafter we refer to as the fitting region) is selected around each identified maximum⁴, always within the wavelength ranges listed in Table 1.
- A straight line is fitted to the data. The result of the fit is taken to be the pseudo-continuum and is used in Eqn. 1.

The wavelength span of the two fitting regions depends on the morphology of the local maxima. On the blue end of the spectrum, where more absorption features are found, the maxima tend to be narrower than on the red end.

⁴ See panel (b) in Fig. 1, the four vertical lines represent an example of the wavelength span of each fitting region.

Thus, the fitting regions are, on average, smaller ($\sim 20 \text{ \AA}$) in the blue and slightly larger ($\sim 25 \text{ \AA}$) in the red part of the spectrum. Larger wavelength spans would tend to set a lower pseudo-continuum level and thus to produce pseudo-EW systematically biased toward smaller values. The size of the fitting region is independent of the signal-to-noise ratio; however, in low signal-to-noise ratio spectra, noise spikes that could bias the pseudo-continuum fit are clipped.

3. Data sets

In the following section, we present the high and low redshift data-sets that we have used in this study.

3.1. High Redshift Data-set

The supernova spectra that are analyzed in this work were obtained as part of several campaigns by the SCP to discover and follow a large number of SNe Ia over a wide range of redshifts (see Lidman et al. (2005) for details). Out of the 20 spectrally confirmed SNe Ia in Lidman et al. (2005), we select the 12 SNe Ia ($z=0.212\text{-}0.912$) with signal-to-noise ratios $S/N > 3$ per 20 \AA bin to pursue our quantitative analysis. One supernova, SN 2001go, was observed at three epochs, so there are 14 spectra in total.

The biases affecting this sample are complex. First, supernova searches are magnitude limited, so Malmquist and light curve shape biases (i.e. brighter/dimmer SN Ia have broader/narrower light curves) make it unlikely that low-luminosity, SN 1991bg-like SNe Ia will be found. Also, it is likely that, while ranking supernovae candidates for follow-up spectroscopy, 1991bg-like SNe Ia would be assigned lower priority due to their low luminosity. Second, it is more difficult to spectrally confirm high-redshift SNe Ia in spectra where host galaxy contamination is above 75% (Lidman et al. 2005; Howell et al. 2005). Although this affects all SNe Ia to some degree, lower-luminosity SNe Ia are more commonly found in bright ellipticals. Moreover, we can not exclude that the signal-to-noise cut we performed while choosing the sub-sample of spectra to study did not introduce an extra selection bias toward over-luminous objects. As it will be clear in section 4, the spectral indicators we use to search for evolution with redshift do not unambiguously discern between normal and over-luminous SN Ia. The additional scatter that would be introduced by using data with lower signal-to-noise ratios would obfuscate the result. We make no attempt to correct the sample for these biases.

The spectra, re-binned to 20 \AA are shown in Fig. 2, and are summarized in Table 2. A full description of the observations and the data reduction are given in Lidman et al. (2005). For each supernova, we use the error spectrum, which was estimated from regions free of SN Ia and host galaxy light on the sky-subtracted two dimensional spectrum, to estimate the statistical uncertainties on the quantities we compute in the following analysis.

High-redshift supernova spectra can contain significant amounts of light from the host galaxy. On the 2d spectra, the host galaxy and the SN Ia are often spatially unresolved, making it difficult to estimate the contribution of the host to the observed flux. We estimated this contribution using a template matching technique based on a large set of nearby supernovae spectra and galaxy models similar to those used in Lidman et al. (2005). The contribution of the galaxy light, relative to the total observed flux, are tabulated in column 10 of Table 2.

The epochs with respect to the B -band maximum light were estimated using the preliminary light curves, if available, and/or spectroscopic dating by template matching with low- z SNe Ia (Lidman et al. 2005; Hook et al. 2005). The two methods usually agree within three days (Hook et al. 2005; Howell et al. 2005), therefore we take 3 days to be the uncertainty on the quoted epoch whenever a light curve estimate of the maximum was not available. The redshift of the supernova, when quoted with 3 significant figures, was estimated from host galaxy lines visible in the spectrum. When this was not possible, the redshift was estimated from supernova spectral features, and is then quoted with 2 significant figures to account for the large intrinsic width of SN Ia spectral features.

3.2. SN Ia identification

The identification of SN Ia relies primarily on the detection of the absorption feature at approximately 6150 \AA due to Si II $\lambda 6355$. At redshifts above $z=0.5$, however, this characteristic feature is redshifted beyond the wavelength range of most optical spectrographs and the classification of the supernova has to rely on spectral features that lie at bluer wavelengths (Lidman et al. 2005; Hook et al. 2005; Matheson et al. 2005). Because of the low signal-to-noise ratio usually available in high-redshift supernova spectra, this approach is not always conclusive.

We can also use the spectra to identify spectral peculiarities among SNe Ia as those found in 91T-like or 91bg-like supernova. In Table 3, the characteristics of four wavelength regions for different types and sub-types of supernovae are schematically reported. Each spectral feature is qualitatively described as *strong*, *weak* or *absent* based on the absorption strength and *broad* or *narrow* based on the wavelength span. In the absence of a procedure that is based on quantitative measurements, this scheme helps in identifying the SN type and, in the case of SNe Ia, the sub-type.

3.3. SN 2002fd: A SN 1991T/SN 1999aa-like Supernova

SN 2002fd ($z = 0.279$) is the only supernova in our data set that clearly deviates from a “normal Ia” (see Table 3). Within the scheme described above, the spectrum of SN 2002fd is similar to the spectra of SN 1999aa (Garavini et al. 2004), a 91T-like supernovae (Fig.3). The

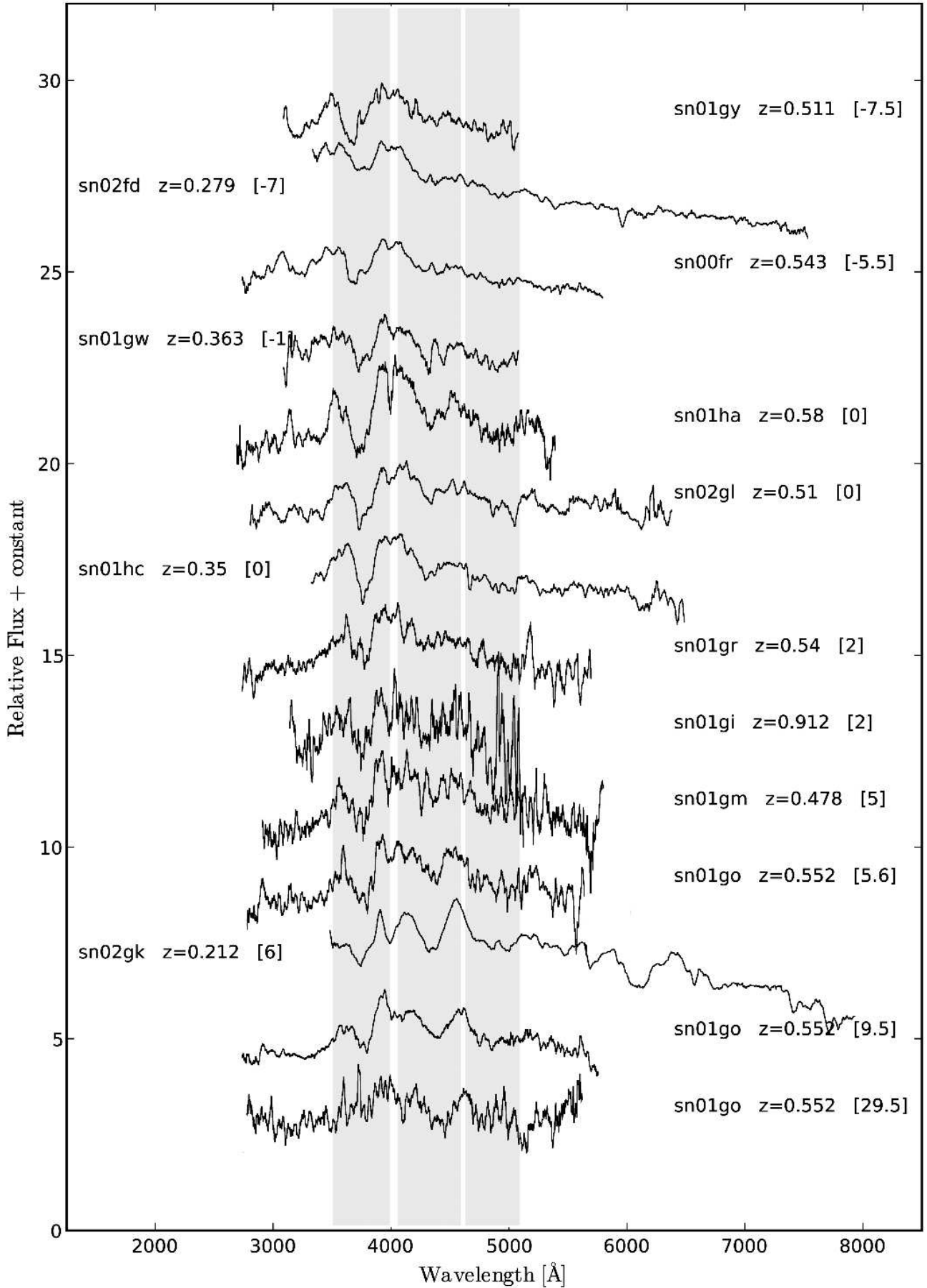


Fig. 2 Spectra of the high-redshift SNe Ia (re-binned to 20 \AA) used in this study, plotted in rest frame. For each spectrum, we indicate the redshift and epoch (in days from B-band maximum; square brackets). See Table 2 for details. Gray vertical bands approximately indicate the wavelength regions used for the quantitative comparison presented in section 4.

Table 2 A summary of the high-redshift data. (See text for details.)

SN-name	Redshift ^a	Date (MJD)	Days from ^b B-band Maximum	Instrument	setup	telescope	Exposure time (s)	S/N ^c	Galaxy ^d %
SN 2001gy	0.511	52021.3	-7,5(1)	FORS1	300V grism + GG435	VLT-UT1	2400	11	20
SN 2002fd ^e	0.279	52376.1	-7(3)	FORS2	300V grism + GG435	VLT-UT4	600	46	28
SN 2000fr	0.543	51676.2	-5.5(1)	FORS1	300V grism + GG435	VLT-UT1	7200	21	16
SN 2001gw	0.363	52021.4	-1(3)	FORS1	300V grism + GG435	VLT-UT1	1200	8	19
SN 2001ha	0.58	52022.0	0(3)	FORS1	300V grism + GG435	VLT-UT1	3600	4	6
SN 2002gl	0.510	52413.1	0(3)	FORS2	300V grism + GG435	VLT-UT4	3000	9	23
SN 2001hc	0.35	52022.1	0(3)	FORS1	300V grism + GG435	VLT-UT1	1800	14	14
SN 2001gr	0.540	52021.0	2(3)	FORS1	300V grism + GG435	VLT-UT1	3600	5	57
SN 2002gi	0.912	52407.2	2(3)	FORS1	300I grism + OG590	VLT-UT3	7200	3	37
SN 2001gm	0.478	52021.3	5(3)	FORS1	300V grism + GG435	VLT-UT1	2400	3	28
SN 2001go	0.552	52021.3	5.6(1)	FORS1	300V grism + GG435	VLT-UT1	2400	5	13
SN 2002gk	0.212	52413.3	6(3)	FORS2	300V grism + GG435	VLT-UT4	900	34	66
SN 2001go	0.552	52027.1	9.5(1)	FORS1	300V grism + GG435	VLT-UT1	7200	10	19
SN 2001go	0.552	52058.1	29.5(1)	FORS1	300V grism + GG435	VLT-UT1	9000	4	53

^aThe redshift is quoted to three significant figures if it is determined from host galaxy lines; two significant figures when determined from SN Ia spectral features.

^bUncertainties are quoted in parentheses. When the epoch is quoted with 3 days uncertainty it refers to that of the best matching low-*z* Ia template.

^cper 20 Å bin

^dEstimated fraction of the galaxy light in the SN Ia spectrum, expressed as percentage of the total flux.

^e 91T-like Type Ia SN

Table 3 A description of the spectroscopic features used to type SN Ia at $z \geq 0.5$. Four wavelength regions are selected for performing the SN Ia typing. See the text for details.

Region Id	λ -Region Rest Frame[Å]	Normal Type Ia	91T/99aa-like	91bg/86G-like	Type Ib/c
‘Ca II H&K’ ^a	3550-3950	strong/broad	weak or absent/broad ^{b,c}	strong/broad	evident/broad ^d
‘Si II’ ^e	3950-4100	evident/narrow ^c	weak ^{b,c}	absent	absent
‘Fe II’ ^{f,g}	4600-5200	strong/broad	strong/narrow ^b	strong/broad	strong/broad
‘S II W’	5200-5600	strong/narrow ^{b,c}	weak or absent ^b	strong/narrow ^{b,c}	absent

^aHigh and low velocity component in some SNe Ia.

^bAround 1 week before maximum light

^cAround maximum light

^dA few exceptions.

^eMarks the beginning of the distinctive strong Ti II absorption feature in 91bg-like SNe Ia.

^fIn Normal Ia characteristic line profile time evolution.

^gDominated by Fe III in pre-maximum spectra of 91T-like SNe Ia.

strength of the ‘Ca II H&K’ feature in SN 2002fd is stronger than in 91T-like SNe Ia and weaker than in normal SNe Ia. The ‘Fe II’ and ‘S II W’ regions are similar to those in SN 1999ac (Garavini et al. 2005). Given the low-redshift, Si II λ 6355 is also visible. This feature in SN 2002fd is intermediate in strength compared with SN 1999aa and in normal SNe Ia. From this qualitative analysis of the spectrum, we classify SN 2002fd as a peculiar SN Ia, similar to the 91T-like SN 1999aa. In section

4.3, we show that the pseudo-equivalent widths of the absorption features in SN 2002fd are also consistent with those found at low redshift for the 91T-like objects.

Finding SNe Ia with spectral characteristics similar to those of SN 1991T at high redshifts is important. The lack of such SNe in high redshift surveys might be a sign of evolution. In a distance limited survey, Li et al. (2001b) found that approximately 20% of the analyzed data set of nearby SNe Ia could be classified

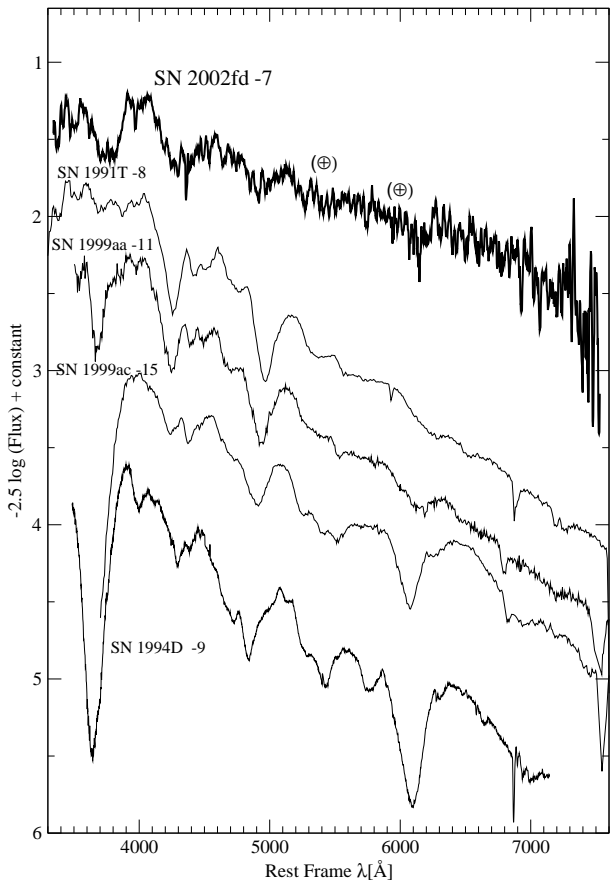


Fig. 3 SN 2002fd at day -7 , re-binned to 20 \AA per pixel (thick solid line), compared to normal and peculiar SNe Ia. The \oplus symbols mark regions of strong telluric absorption.

as SN 1991T/SN 1999aa-like which were peculiar, over-luminous SNe Ia (Garavini et al. 2004). This percentage is probably higher than that of peculiar 91T-like found at high-redshift. Currently, the reported fraction of 91T-like SNe Ia is $\leq 5\%$ (Lidman et al. 2005; Matheson et al. 2005). However, the fraction of these SNe Ia in high-redshift surveys is uncertain because of the difficulty in identifying such SNe Ia. Several more 91T-like SNe Ia may have already been observed at high-redshift but not clearly identified because the spectrum was taken well after maximum light or the light-curve had a Δm_{15} consistent with normal SNe Ia. Over-luminous SNe Ia such as 91T-like SNe Ia generally have broader light-curves than normal SNe Ia. However, it is now becoming evident that 91T-like SNe Ia do not always have high Δm_{15} values and that broad light-curve SNe Ia do not always show the spectra peculiarities seen in 91T-like SNe Ia. Example of the latter case are SN 1999ee (Hamuy et al. 2002), SN 2002cx (Li et al. 2003) or SN 1999aw (Strolger et al. 2002). Li et al. (2001a) computed that the peculiarity rate for 91T-like SNe Ia should vary between 6% and 18.6%. In this case the observed peculiarity rate at high redshift (about 4% in Matheson et al. (2005) and about 5% in our data set) is consistent with the computations, especially if one considers that the expected number of pecu-

liar supernovae is highly dependent on the search strategy. Nevertheless, the identification of peculiar SNe Ia in high-redshift samples is an important step toward determining whether the range of SNe Ia sub-types that is observed at low redshift is also observed at high redshifts. Of course, large data samples with high signal-to-noise ratio spectra are required to check whether the fraction of peculiar high-redshift SNe Ia is consistent with that found in the low-redshift Universe or if there is an evolution with redshift in the relative fractions, which might affect the derivation of cosmological parameters from SNe Ia.

3.4. Nearby Supernova Data-sets

Two different data sets are used to derive the properties of pseudo-EW in local SNe Ia.

Set A - 77 spectra (presented in Folatelli (2004)) from 13 of the SNe Ia discovered and followed by the Supernova Cosmology Project (SCP) in collaboration with members of the EROS (Hardin et al. 2000), QUEST (Schaefer et al. 1999), and Nearby Galaxies SN Search (Gal-Yam et al. 1999) teams. The redshift range of these SNe Ia is $0.01 < z < 0.15$.

The two-dimensional raw images were reduced according to standard procedures. The calibrated spectra were additionally corrected for atmospheric and Galactic extinction (Cardelli et al. 1989; Schlegel et al. 1998) and their flux-calibration was checked against measured broad-band photometry and found in agreement within the quoted uncertainties. The spectra were de-redshifted. More details about these data can be found in Table 4. All the spectra in **Set A** include estimated statistical uncertainties for each wavelength bin. Host-galaxy light was present in a subset of these spectra. This contribution was estimated and subtracted (for details on the procedure see Sec. 3.1) in those cases where it exceeded 10% of the total flux.

Set B - 89 published spectra from 8 well-observed, nearby objects (see Table 5). Additionally, the spectra were scaled to match the photometry. Given the absence of published uncertainties on these spectra, statistical errors were estimated from the pixel-to-pixel variation.

The epochs used in this analysis are based on light curve estimates. In the case of **Set A**, the date of maximum B -band brightness was determined using preliminary light curves. Therefore the epochs used to date the spectra were taken as the integer number of days since maximum light. The photometric data available for both sets were used to fit the template B -band light curve given by Goldhaber et al. (2001) and thus to obtain the values of the light curve decline parameters $\Delta m_{15}(B)$ and stretch (s) for each SN Ia.

The two sets contain some peculiar SNe Ia, including the prototypes of the two subclasses: SN 1991T and SN 1991bg. SN 1999aa (Garavini et al. 2004), SN 1999aw (Strolger et al. 2002), and SN 1999bp (Folatelli 2004) are included in the 1991T-like subclass. All these SNe Ia

Table 4 SNe Ia from **Set A** (SCP data: Folatelli (2004)).

SN	z	Host Galaxy	Galaxy Type ^a	Rest-Frame Spectral Epochs ^b
1999aa	0.0144	NGC 2595	SAB(rs)c	-11, -7, -3, -1, 5, 6, 14, 19, 25, 28, 33, 40, 47, 51, 58
1999ac	0.0095	NGC 6063	Scd	-15, -9, 0, 2, 8, 11, 16, 24, 28, 31, 33, 39, 42
1999ao	0.054	Anon.	S:	5, 7, 10, 13, 18, 34, 40
1999au	0.124	Anon.	S:	12, 17
1999av	0.05	Anon.	E/S0:	2, 5, 9, 31
1999aw	0.038	Anon.	(?)	3, 5, 9, 12, 16, 24, 31, 38
1999be	0.019	Anon.	(?)	14, 19, 26, 33, 37, 44
1999bk	0.096	Anon.	E/S0:	4, 7, 9
1999bm	0.143	Anon.	S:	3, 6, 21
1999bn	0.129	Anon.	S:	2, 14, 22
1999bp	0.077	Anon.	S:	-2, 0, 1, 6, 17, 23
1999bq	0.149	Anon.	E/S0:	3, 18
1999by	0.0021	NGC 2841	SA(r)b	1, 6, 16, 27, 34

^a Hubble type of the host galaxy. An entry followed by a colon is a classification based on the host galaxy spectrum. The rest are taken from NED⁵

^b Rest-frame days since B -band maximum light.

Table 5 SNe Ia from **Set B** (Public data).

SN	z	Host Galaxy	Galaxy Type ^a	Rest-Frame Spectral Epochs ^b	References
1981B	0.0060	NGC 4536	SAB(rs)bc	0, 17, 26, 29, 35, 49	1
1986G	0.0018	NGC 5128	S0 pec	-7, -5, -1, 0, 3, 21, 28, 41, 44, 55	2
1989B	0.0024	NGC 3627	SAB(s)b	-7, -5, -3, -2, -1, 3, 5, 8, 9, 11, 16, 18, 19	3
1990N	0.0034	NGC 4639	SAB(rs)bc	-14, -7, 7, 14, 17, 38	4, 5, 6
1991bg	0.0035	NGC 4374	E1	-2, 0, 13, 16, 23, 24, 30, 31, 44, 52	7, 8
1991T	0.0058	NGC 4527	SAB(s)bc	-11, -9, -8, -7, -6, -5, -3, 0, 10, 15, 23, 24, 42, 45	9, 10, 11, 12
1992A	0.0063	NGC 1380	SA0	-5, -1, 3, 7, 9, 11, 16, 17, 24, 28, 37, 46	13
1994D	0.0015	NGC 4526	SAB(s)	-10, -9, -8, -7, -5, -3, 2, 4, 6, 8, 11, 13, 14, 16, 18, 20, 25	14, 15

^a Hubble type of the host galaxy from NED⁵.

^b Rest-frame days since B -band maximum light.

Sources: (1) Branch et al. (1983); (2) Phillips et al. (1987); (3) Wells et al. (1994); (4) Leibundgut et al. (1991); (5) Phillips et al. (1992); (6) Mazzali et al. (1993); (7) Filippenko et al. (1992a); (8) Leibundgut et al. (1993); (9) Filippenko et al. (1992b); (10) Ruiz-Lapuente et al. (1992); (11) Phillips et al. (1992); (12) Jeffery et al. (1992); (13) Kirshner et al. (1993); (14) Meikle et al. (1996); (15) Patat et al. (1996).

present values of the decline rate parameter $\Delta m_{15}(B) < 1.0$ ($s > 1.1$) and thus have a slow post-maximum decline in luminosity. At the other extreme, SN 1986G (Phillips et al. 1987; Cristiani et al. 1992) and SN 1999by (Vinkó et al. 2001; Garnavich et al. 2004) belong to the 1991bg-like subclass. These are fast-declining SNe Ia, with $\Delta m_{15}(B) > 1.70$ ($s < 0.80$). The case of SN 1999ac (Garavini et al. 2005) is considered separately. This SN Ia has photometric and spectroscopic peculiarities that make it a unique object: its light curve shows a slow rise similar to SN 1991T but a fast decline (Phillips et al. 2002) and its spectrum is similar to SN 1999aa.

⁵ The NASA/IPAC Extragalactic Database (NED) is operated by the Jet Propulsion Laboratory, California Institute of Technology, under contract with the National Aeronautics and Space Administration.

4. Results

We first perform a qualitative analysis (sections 4.1 and 4.2) and then turn to a more quantitative approach (sections 4.3 and 4.4).

4.1. Absorption Velocities

For normal SNe Ia, the magnitude of the blueshift of the Ca II H&K absorption minimum drops rapidly, from values around 22000 km/s before maximum light to 14000 km/s at maximum light. After maximum light, the decline in velocity flattens and decreases by about 4000 km/s in 50 days. The mean trend for normal SNe Ia, from 10 days before maximum light to 40 days after maximum light, is shown in Fig. 4 together with the evolution in the velocities of fast and slow-declining local SNe Ia. The shaded area represents the 1

σ dispersion about the mean for normal SNe Ia. The trend and the dispersion have been computed from a large sample of nearby supernova (Garavini et al. 2004).

The measured absorption velocity of the ejecta in under-luminous SNe Ia (i.e. SN 1999by and SN 1991bg plotted with the dotted and dashed lines, respectively) is approximately 1.5 σ lower than the mean absorption velocity in normal SNe Ia. Therefore, the measurement of a low blueshift of the Ca II H&K absorption minimum cannot be used to identify a SNe Ia as under-luminous as already pointed out in Blondin et al. (2006). Peculiar over-luminous SNe Ia such as SN 1991T and SN 1999aa show blueshifts of Ca II H&K absorption minimum that are within one σ of those of normal SNe Ia. SN 1991T at one day before maximum light shows a blueshifts comparable with that of SN 1999by, a fast-declining SN Ia.

In Fig. 4, the velocities of both the low-redshift and high-redshift SNe Ia are individually measured by performing an error-weighted non-linear least-squares fit to the entire line profile, manually selecting the end points limiting the wavelength region where to perform the fit. The line profile is modeled with a Gaussian plus a linear component. This method accurately reproduces the absorption line profile and it has been successfully used in previous studies (e.g. Garavini et al. (2005); Hook et al. (2005)). All the SNe Ia in our data set were measured (Table 6), with the exception of SN 2001gk, for which the line profile is incomplete, and SN 2001go at +29 days, for which the signal-to-noise is too low to correctly identify the absorption. The uncertainty in the redshifts is taken to be $\sigma_{cz} = 300 \text{ km/s}$ if the redshift was estimated from galaxy lines. For SN 2001ha and SN 2001hc, we could not identify host galaxy lines, so their redshifts were estimated by comparing their spectra with the spectra of nearby SNe Ia (Lidman et al. 2005). In these cases the uncertainty is increased to $\sigma_z = 0.01 \equiv \sigma_{cz} = 3000 \text{ km/s}$. This uncertainty dominates the statistical uncertainty from the fit. We note that the velocities of our high-redshift SNe Ia are consistent with the main trend of spectroscopically normal local SNe Ia. In Fig 4 open circles indicate the measurements reported in Hook et al. (2005) where a similar result was found in an independent sample of high redshift SNe Ia.

4.2. Pseudo-Equivalent Widths

Given the mean redshift of the high-redshift sample ($z=0.49$) and the typical S/N ratio of the spectra, we restrict our analysis to the bluest and strongest features - #4 “Fe II 4800”, #3 “Mg II 4300” and #1 “Ca II H&K”.

4.2.1. Estimating Systematic Errors

Possible systematic errors arising from the choice of the fitting region at either side of the feature where the pseudo-continuum is fitted were accounted for by randomly shifting these regions (typically within a third of the region

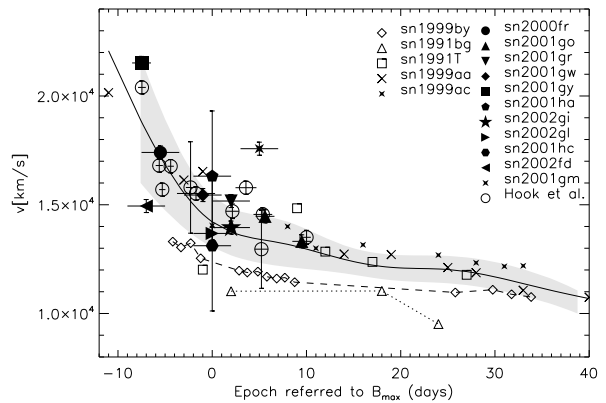


Fig. 4 The change in the blueshifts of the Ca II H&K absorption minimum with epoch for a sample of high-redshift SNe Ia (presented in section 3, filled symbols, and from Hook et al. (2005) open circles) and a sample of low-redshift SNe Ia. The dashed and dotted lines indicate the values of extremely under-luminous SNe Ia SN 1999by (Garnavich et al. 2004) and SN 1991bg (Leibundgut et al. 1993) respectively. The solid line indicates the average trend for Ca II H&K, which has been computed using a large data set of low-redshift normal SNe Ia (Garavini et al. 2004). The gray band shows the dispersion (1 standard deviation) of the data about the average trend.

size in each direction⁶) and computing the weighted root-mean square deviation (rms) of the measured pseudo-EWs. This was the dominant source of uncertainties when the signal-to-noise ratio per resolution element was above ~ 10 . Additionally, for lower signal-to-noise spectra (specifically in the case of our high redshift data-set) the central wavelength of the fitting region was randomly shifted according to a Gaussian distribution with $\sigma=10\text{\AA}$. The change in the pseudo-EW is insignificant for high signal-to-noise ratio data. The standard deviations of these distributions were chosen in a conservative manner so as to take into account even large systematic effects. This source of error was added quadratically to the one given in Eqn. 2.

It is known that pseudo-EWs can be affected by poor resolution and low signal-to-noise ratios (see, for example Gray (1992)). Both effects were tested. Boxcar smoothing was used to decrease the resolution of the best-sampled spectra ($\sim 10 \text{ \AA}/\text{pixel}$) so that the range of resolutions in the present data set were tested. Due to the large intrinsic width of the broad SN Ia features, no significant change in the measured pseudo-EW was found.

Signal-to-noise ratios ranged from about 5 to several hundred. When Gaussian noise was added to the best-quality spectra, in order to reproduce that quality range,

⁶ Considering the uncertainty on the location of a region of size l to be $l/\sqrt{12} \sim l/3$, as derived from the second moment of a uniform distribution.

Table 6 Magnitude of the blueshift of Ca II H&K absorption minimum. Measurement uncertainties are reported in parenthesis.

SN	day	vel [km s ⁻¹]
sn2001gy	-7.5 (1)	21520 (300)
sn2002fd	-7 (2)	14940 (300)
sn2000fr	-5.5 (1)	17400 (300)
sn2001gw	-1 (2)	15440 (300)
sn2002gl	0 (2)	13680 (300)
sn2001ha	0 (2)	16310 (3000)
sn2001hc	0 (2)	13110 (3000)
sn2002gi	2 (2)	13950 (300)
sn2001gr	2 (2)	15170 (300)
sn2001gm	5 (2)	17580 (300)
sn2001go	5.6 (1)	14470 (300)
sn2001go	9.5 (1)	13320 (300)

no significant bias was detected in the resulting pseudo-EWs.

Additionally, the effect of reddening was tested by artificially adding up to $E_{B-V} = 0.32$ magnitudes of reddening (corresponding to $A_V = 1$ mag, with $R_V = 3.1$) following the law given in Cardelli et al. (1989). This produced no significant change in the resulting pseudo-EWs. This is expected since the pseudo-EWs are defined over a limited wavelength range.

Further systematic effects could arise from host-galaxy light that has not been perfectly removed. The effect of additional signal underlying the SN Ia spectrum would be to lower the pseudo-EW. The spectra from **Set B** in the present sample correspond to very bright, nearby SNe Ia, for which SN Ia and host-galaxy spectra can be resolved. For more distant SNe Ia, from **Set A** and the high redshift data set, the light from the host can contribute up to 50% of the light in the extracted spectra. We have tested how errors in estimating the amount of host galaxy light can affect the pseudo-EWs of a typical near-maximum light SNe Ia spectrum. Template galaxy spectra of Hubble types E and Sc were added to the SN Ia spectrum in order to simulate contamination levels ranging up to 50% of the total integrated flux between 3500 and 9000 Å. The pseudo-EWs of the features were then measured on every spectrum. The relative decrease in the pseudo-EW with increasing contamination levels was found to be approximately linear. Table 7 summarizes these results by giving the relative decrease in the pseudo-EW per each 10% of unaccounted contamination on the total integrated flux for both galaxy types. Since SNe Ia near maximum light are generally bluer than their hosts, errors in estimating the amount of host galaxy contamination leads to larger errors in the pseudo-EWs for features at redder wavelengths. For early type galaxies, because of the presence of the Balmer break around 4000Å, the effect on the pseudo-EW of “Ca II H&K” is less than 10% even for 50% contamination.

Table 7 The fractional decrease in the pseudo-EW corresponding to a 10% increase in the amount of contamination from the host.

Feature ID	Mnemonic Label	Host Type	
		E ^a	Sc ^a
1	“Ca II H&K”	0.019	0.080
2	“Si II 4000”	0.048	0.074
3	“Mg II 4300”	0.037	0.073
4	“Fe II 4800”	0.070	0.074
5	“S II W”	0.112	0.074
6	“Si II 5800”	0.128	0.066
7	“Si II 6150”	0.103	0.084
8	“Ca II IR”	0.155	0.114

^a Fractional decrease in pseudo-EW.

4.2.2. “Fe II 4800” (#4).

The evolution in the pseudo-EW of feature #4, “Fe II 4800”, in nearby supernovae is shown in Fig. 5. The number of data points enable us to compute a mean trend, which is shown as the solid line in Fig. 5, for normal SNe Ia only. The curve was built in the range $-10d < \text{epoch} < 50d$ by dividing the epochs into 5 bins, calculating a weighted average of the pseudo-EW in each bin, and finally tracing the spline function through those points as a general indication of the followed time evolution. The coordinates (epoch, pseudo-EW), in units of days and Å, of the 5 points defining the curve are: (-5,134); (5,181); (15,267); (25,339); (35,356).

The pseudo-EW of “Fe II 4800” monotonically increases with phase from before maximum light to about 30 days after maximum light. This is due to the increasing optical depth of Fe II lines from around maximum light onward and to the subsequent overlapping of several Fe II lines from around 15 days after maximum light (see Fig. 1).

The evolution of pseudo-EWs is similar for all Ia subtypes, but offset from the mean curve. In general, 1991bg-like SNe Ia lie above the curve and 1991T-like SNe Ia lie below it but there is no firm correlation with Δm_{15} . This is summarized in Table 8 which shows the distribution

of the three SNe Ia subtypes with respect to the average curve.

We note that for normal type Ia SNe the average trend in the first data bin is based on four data points from SN 1994D and one each from SN 1989B and SN 1990N. The mean is then biased toward the average pseudo-EW value of SN 1994D between -10 and -6 days. This is higher than the measurement obtained on the other SNe Ia, thus, the pre-maximum average trend is biased toward the trend observed in SN 1994D. More pseudo-EW measurements are needed to firmly establish the pre-maximum evolution in normal SNe Ia.

In Fig 5 (lower panel) the “Fe II 4800” pseudo-EWs of the high redshift sample are shown. All SNe Ia (with the exception of SN 2001gu, SN 2001gw, SN 2001gy and SN 2002gi, for which the absorption feature was not easily identifiable) were found to lie within the 95% probability distribution of low-redshift supernovae indicated by the gray filled area.

4.2.3. “Mg II 4300” (#3)

Various ions correspond to feature #3. These include Mg II, Co II, Fe II, Fe III, and Si III for spectroscopically normal and 1991T-like SNe Ia. In the case of 1991bg-like SNe Ia, the region is dominated by strong lines of Ti II (Filippenko et al. 1992a; Mazzali et al. 1997). The evolution of the pseudo-equivalent width of this feature is different than that of “Fe II 4800” as can be seen in Fig. 6.

The pseudo-EW of the feature increases dramatically over a short period of time as it merges with the neighboring “Si II 4000” feature (feature #3 in figure 6). Before and after this increase, the pseudo-EW of this feature is approximately constant. The phase at which this increase takes place, t_{br} , is highly dependent on the SN Ia subtype. For 1991bg-like SNe Ia it seems to occur as early as 5 days before maximum light (the earliest spectrum of a 1991bg-like SN Ia in our sample), while normal SNe Ia show this behavior around one week after maximum light, and 1991T-like objects show it later than day +10. Thus, the evolution of the pseudo-EW of the “Mg II 4300” feature can be used to discriminate between different Type Ia subtypes.

We describe the average evolution of this feature with the function:

$$f(\theta, t) = \frac{A}{e^{\frac{t_{br}-t}{\tau}} + 1} + B, \quad (3)$$

with parameters $\theta = (A, B, t_{br}, \tau)$. Parameters (A, B) are simple constants, t is the SN phase, and τ is an e-folding time scale. The solid line in Fig. 6 shows the average curve for normal SNe Ia between days -10 and +30. Other SN Ia subtypes show a parallel trend. Table 9 lists the dispersion of normal SNe Ia around the average curve and the deviations of 1991T-like and 1991bg-like SNe Ia from the same curve. The parameterization introduced in Eq. 3 allows one to quantify the sudden change in the

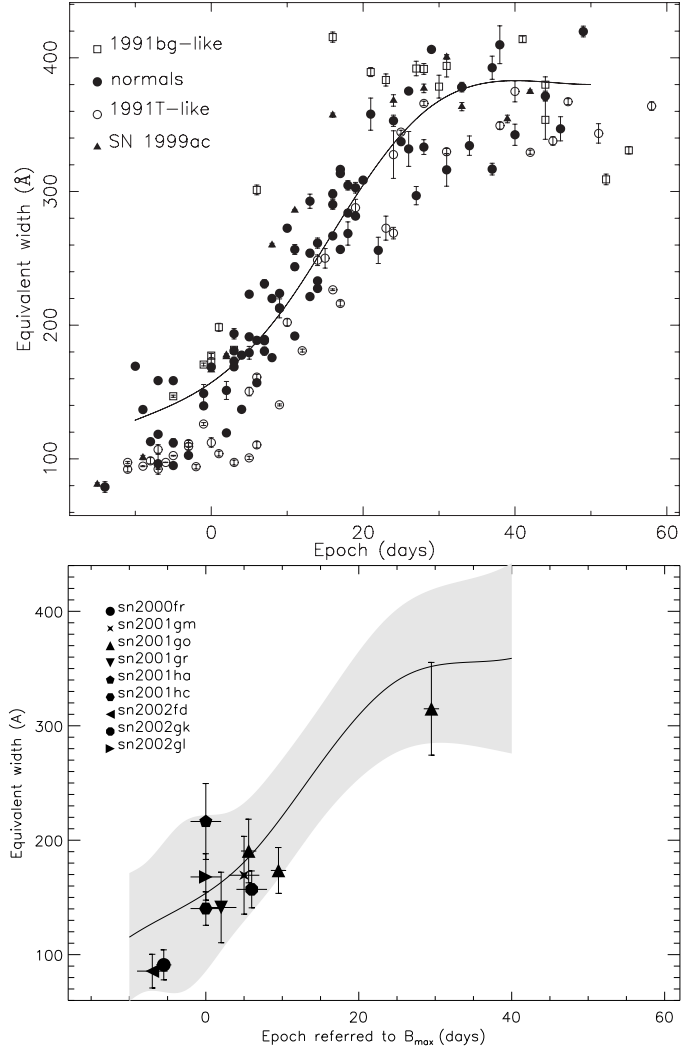


Fig 5

“Fe II 4800”

Upper Panel: Measured pseudo-equivalent width corresponding to the “Fe II 4800” feature (#4). SN 1991bg-like objects are marked with open squares, 1991T-like SNe Ia with open circles, normal SNe Ia with filled circles and SN 1999ac with triangles. Error-bars include the error described by Eqn. 2 as well as systematic uncertainties arising from the pseudo-continuum fit. The solid line shows a cubic spline function used to represent the average evolution of normal SNe Ia between days -10 and +50. In general, 1991bg-like SNe Ia lie above the average curve whereas 1991T-like SNe Ia lie below it. *Lower Panel:* A comparison between the ‘Fe II 4800’ pseudo-EWs in low- and high-redshift SNe Ia. High-redshift supernova are indicated by large filled symbols. The gray filled area represents the 95% probability region for normal low-redshift SNe Ia. See text for details.

pseudo-EW in terms of the parameter t_{br} , which can then be used to classify type-Ia supernovae into the three main sub-types. In Fig. 6 (upper panel) we note that, for normal type Ia SNe before maximum light, the pseudo-EW measurements tend to cluster around high and low values. The high values of pseudo-EW are those measured

Table 8 Dispersion of “Fe II 4800” pseudo-EW for the three SNe Ia subtypes. See text for details.

Epoch bin	n	Normal		1991T-like		1991bg-like	
		\langle pseudo-EW \rangle (\AA)	δ (\AA)	n	$\delta_{\text{pseudo-EW}}$ (\AA)	n	$\delta_{\text{pseudo-EW}}$ (\AA)
(1)	(2)	(3)	(4)	(5)	(6)	(7)	(8)
[−10, −6]	6	132 ± 11	28	5	−29 ± 3	0	...
[−5, −1]	6	114 ± 12	37	5	−36 ± 5	2	16 ± 4
[0, 5]	12	164 ± 10	28	5	−62 ± 9	4	24 ± 7
[6, 11]	15	200 ± 8	25	4	−58 ± 15	1	113 ^a
[12, 18]	15	265 ± 9	25	5	−47 ± 12	1	139 ^a
[19, 27]	10	316 ± 12	30	5	−34 ± 18	3	58 ± 8
[28, 40]	9	353 ± 13	36	5	3 ± 9	3	37 ± 5

Columns: (1) Range of epoch bins in days; (2) Number of points from normal SNe Ia; (3) Average pseudo-EW for normal SNe Ia; (4) Dispersion (rms) of normal SNe Ia around the average curve⁷; (5) Number of points from 1991T-like SNe Ia; (6) Mean deviation of 1991T-like SNe Ia from the average curve. Uncertainties do not include the computed dispersion of normal SNe Ia around the curve (δ); (7) Number of points from 1991bg-like SNe Ia; (8) Mean deviation of 1991bg-like SNe Ia from the average curve. Uncertainties do not include the computed dispersion of normal SNe Ia around the curve (δ).

^a Only one measurement, thus no uncertainty is given.

on SN 1989B (two data points in the first epoch bin and three in the second one) and on SN 1990N (one data point in each bin). Instead, SN 1994D shows low pseudo-EWs (two data points in each bin before maximum light), with SN 1992A pseudo-EW having intermediate values (in both pre-maximum bins). The average trend is then greatly affected by SN 1994D which, as for feature #4, seems to be an outlier. Because of the low statistics the pre-maximum trend is only indicative. An analysis including more normal type Ia SN will be needed to assess the average trend and to investigate whether the apparent clustering in the distribution is a distinctive characteristic of type Ia SNe disclosing interesting physics.

From Fig. 6 (upper panel), it is evident that the evolutionary behavior of the “Mg II 4300” pseudo-EW is different for normal, 91T-like, and 91bg-like SNe Ia, and therefore could correlate also with photometric properties of the SN. To quantify this correlation, the functional model given by Eq. 3 was used to fit the parameter t_{br} for each of SN Ia individually. This parameter is related to the phase at which this feature suddenly becomes stronger. Table 10 lists the values of t_{br} for 11 SNe Ia in our sample. In the cases of SN 1991bg and SN 1999by, the epochs of their earliest spectra are used as upper limits for t_{br} , assuming they followed the same evolutionary pattern found for the other objects. The values of $\Delta m_{15}(B)$ were re-fitted for this analysis to gain consistency in the results. Fig. 7 shows the correlation between $\Delta m_{15}(B)$ and t_{br} . The break occurs at later epochs for SNe Ia with slower declining lightcurves. A least-squares fit yields:

$$\Delta m_{15}(B) = 1.869(\pm 0.052) - 0.070(\pm 0.005)t_{br}, \quad (4)$$

⁷ In general we find $\delta \sim \sqrt{N} \cdot \delta_{\text{pseudo-EW}}$, but note that there are slight deviations due to the use of different epoch bins for this table and in building the average trend.

where $1.7 < t_{br} < 16.9$ is given in days since maximum light. The fit was done excluding the two upper limits. The resulting dispersion in $\Delta m_{15}(B)$ around the fitted line is 0.08 mag, which is comparable to the measurement uncertainties. Since this spectral feature is covered by the standard B filter, the correlation is not surprising. The sudden strengthening of the “Mg II 4300” absorption appears to affect the shape of the lightcurve.

An additional point to note is that this feature can be observed with optical spectrographs up to redshifts of ~ 1 , and the technique can be used up to redshifts ≥ 1.7 with future SN-related cosmology experiments (e.g ADEPT, DESTINY or SNAP) which will include near-infrared spectrographs. However, since several spectroscopic observations are needed to obtain the value of t_{br} , the use of this parameter to estimate M_B^{max} would be limited to SNe Ia with rather extensive spectroscopic follow-up.

Fig 6 (lower panel) shows that the “Mg II 4300” pseudo-EWs of the high-redshift supernovae (all except SN 2002gi are measured) are consistent with the trend defined by the 95% probability distribution of low-redshift normal supernova indicated by the gray filled area. Moreover, SN 2001go, for which measurements at three epochs are available, shows the sudden increase at around one week after maximum, as do most low-redshift normal SNe Ia.

4.2.4. “Ca II H&K” (#1)

The prominent absorption trough at 3800\AA is attributed to the Ca II H&K lines with contributions from Si II $\lambda 3858$ and lines from iron-peak elements. Fig. 8 shows the change in the pseudo-EW of this feature with phase. As expected for SN 1991T-like objects, this absorption is particularly weak (low pseudo-EW), especially in the pre-maximum spectra. The intrinsic dispersion in the pseudo-

Table 9 Dispersion of “Mg II 4300” pseudo-EW for the three SN Ia subtypes. See text for details.

Epoch bin	n	Normal		1991T-like		1991bg-like	
		\langle pseudo-EW \rangle (\AA)	δ (\AA)	n	$\delta_{\text{pseudo-EW}}$ (\AA)	n	$\delta_{\text{pseudo-EW}}$ (\AA)
(1)	(2)	(3)	(4)	(5)	(6)	(7)	(8)
[−10, −5]	6	90 ± 7	16	6	15 ± 4	0	...
[−4, 0]	6	98 ± 5	14	5	−5 ± 3	4	139 ± 22
[1, 5]	9	118 ± 12	28	4	−25 ± 12	1	206 ^a
[6, 10]	10	184 ± 14	26	4	−77 ± 12	0	...
[11, 17]	15	251 ± 10	33	5	−69 ± 23	2	48 ± 2
[18, 30]	15	257 ± 7	27	6	8 ± 6	4	21 ± 20

See column explanations in Table 8.

^a Only one measurement, thus no uncertainty is given.

Table 10 $\Delta m_{15}(B)$ and t_{br} measured on the nearby supernova sample.

SN	$\Delta m_{15}(B)$ ^a	t_{br} ^b
1986G	1.73(05)	1.7
1989B	1.32(07)	7.1
1990N	1.03(10)	9.2
1991T	0.96(07)	12.1
1991bg	1.93(05)	< 0 ^c
1992A	1.45(04)	7.0
1994D	1.46(10)	7.0
1999aa	0.95(08)	13.6
1999aw	0.75(10)	16.4
1999bp	0.70(06)	16.9
1999by	1.90(05)	< 1 ^c

^a Uncertainties given between brackets, in units of 0.01 mag.

^b Spectral parameter related to “Mg II 4300” (Eqn. 3). Assumed uncertainty in t_{br} : 0.5d. Measured in days since maximum light.

^c Upper limit corresponding to the earliest data point.

EWs is greater than in the case of features #3 (Mg II 4300) and #4 (Fe II 4800).

This is primarily due to the strength of the Ca II H&K line when compared with Mg II and Fe II. The evolution of the pseudo-EW with phase is specific to each object both qualitatively and quantitatively. The dispersion on pseudo-EW is greater before maximum light, where some objects show an increase and others a decrease. After maximum light, there is normally a slow decrease, except for the 1991bg-like objects in which the pseudo-EW is relatively constant. The spread of pseudo-EWs of this feature is the largest of all the features analyzed in this work. This is due, in part, to the possible presence of high velocity components and to the overlap of several lines that lie in the wide wavelength interval spanned by this feature. As pointed out in Mazzali et al. (2005) the position in velocity space of such components differ in different SNe Ia making the feature broader or narrower and thus affecting the measured pseudo-EW.

The two points with pseudo-EW > 170 \AA after day 0 belong to SN 1999bm. Their large pseudo-EW values are due to an unusually broad “Ca II H&K” feature. As pointed out in Gerardy et al. (2004) this phenomenon might be

caused either by the presence of a strong, high-velocity Ca II component or by a strong Si II 3858 line. Disentangle between these two hypotheses is difficult. The presence of a high-velocity Ca II component could be better determined in the Ca II IR triplet region, because of the lack of contamination from other ions. However, in our spectra of SN 1999bm the signal-to-noise around 8000 \AA is too low to identify such component. It is impossible to exclude an high-velocity component based only on Ca II H&K. The strength of the Ca II H&K line could result in a single minimum absorption line even when an high-velocity components is present and detected in the Ca II IR triplet.

The pseudo-EW of “Ca II H&K” feature of low- and high-redshift supernova are shown in Fig. 8. For this feature, as described above, it is not possible to identify a distinctive trend for SN Ia subgroups as a function of time. Before twenty days past maximum, normal and under-luminous low-redshift SNe Ia populate the region that spans from pseudo-EW $\bar{60}$ \AA to pseudo-EW $\bar{140}$ \AA . In the lower panel of Fig. 8, the gray filled area represents the 95% probability region for normal (non-outliers) and under-luminous low-redshift SNe Ia. Some outliers (determined by a 3-sigma clipping algorithm) are found among

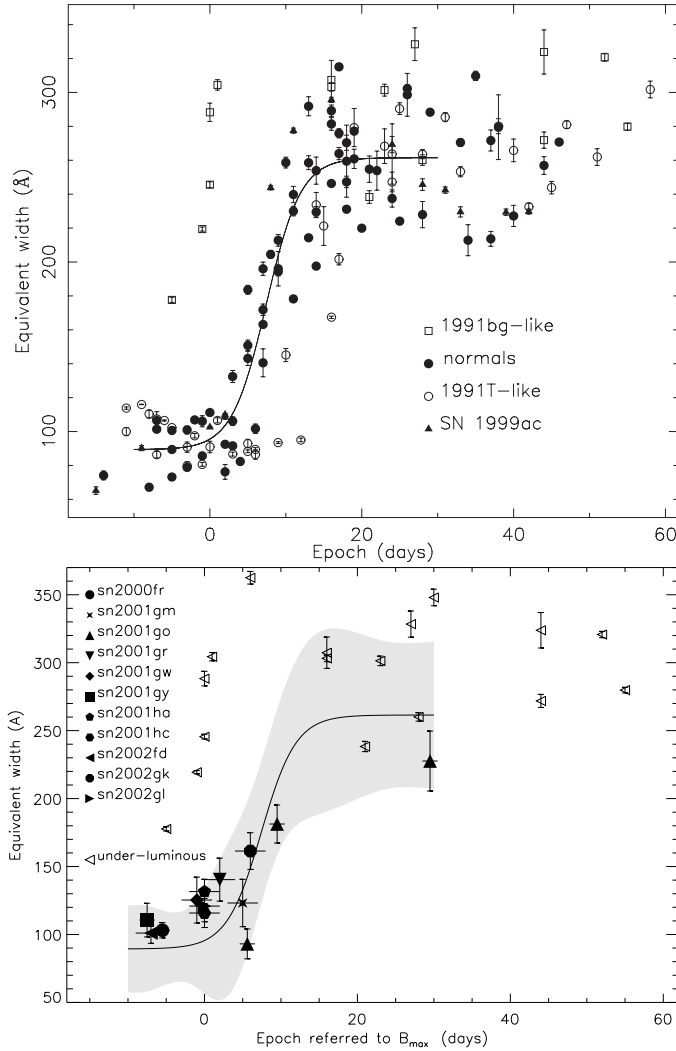


Fig. 6 “Mg II 4300”
Upper Panel: Measured pseudo-equivalent widths corresponding to “Mg II 4300” (#3). SN 1991bg-like objects are marked with open squares, 1991T-like SNe Ia with open circles, normal SNe Ia with filled circles and SN 1999ac with triangles. Error-bars include the error described by Eqn. 2 as well as systematic uncertainties arising from the pseudo-continuum fit. The solid line represents the average behavior of normal SNe Ia, as described in Eqn. 3 with $\theta=(172.2, 89.4, 7.5, 2.5)$. In general, 1991bg-like SNe Ia lie above the average curve whereas 1991T-like SNe Ia lie below it. *Lower Panel:* A comparison between the ‘Mg II 4300’ pseudo-EWs in low- and high-redshift SNe Ia. High-redshift supernova are indicated by large filled symbols. The gray filled area represents the 95% probability region for normal low-redshift SNe Ia. Peculiar under-luminous nearby SNe Ia are shown separately for comparison. See text for details.

normal SNe Ia and are indicated with small diamond symbols. Before maximum light, peculiar 91T-like objects show systematically low values, as indicated by the small square symbols. The high-redshift supernovae (all except SN 2002gi are plotted) do not show significant deviations

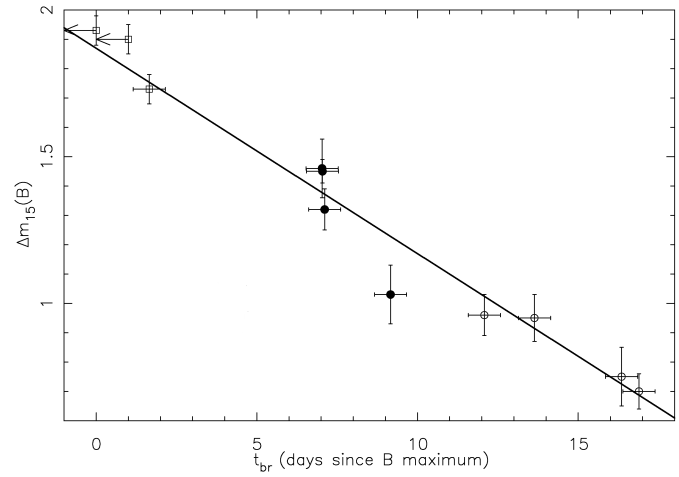


Fig. 7 The “Mg II 4300” pseudo-EW break parameter t_{br} (Eqn. 3). $\Delta m_{15}(B)$ versus t_{br} . The two points marked with arrows correspond to upper limits of t_{br} . The straight line is least-squares fit to the data, excluding the upper limits.

with respect to the low-redshift sample shown in the plot, and SN 2002fd falls on the 91T-like trend as expected.

4.3. The “Ca II H&K” pseudo-EW of SN 2002fd

Prior to maximum light, the pseudo-EW of Ca II H&K can be used to separate 91T-like SN Ia from normal SNe Ia, (see Fig. 8). If the identification of SN 2002fd as a peculiar object is correct, we expect the pseudo-EW to be lower than that of normal SNe Ia. The average pseudo-EW prior to maximum light in normal SNe Ia is $\langle \text{pseudo-EW} \rangle = 114.1$ and the scatter around the mean value is $\sigma_{\langle \text{pseudo-EW} \rangle} = 14.2$. For peculiar 91T-like SNe Ia we find $\langle \text{pseudo-EW} \rangle = 68.7$ and $\sigma_{\langle \text{pseudo-EW} \rangle} = 6.1$. The value measured for SN 2002fd, (pseudo-EW = 73.6 ± 2.9), is consistent — within one standard deviation — with that found for 91T-like SN Ia, and inconsistent (at more than 3 standard deviations) with normal SNe Ia.

Note, that the plotted errors bars in the pseudo-EWs of the high-redshift SNe Ia include both statistical uncertainties, from the measurement, and systematic uncertainties from residual host galaxy contamination but do not include systematic uncertainties from possible misidentification of the maxima around the absorption feature (i.e. misidentification of the fitting regions). Table 11 reports the measured pseudo-EWs.

4.4. Statistical comparison

In this section, a statistical comparison of the low- and high-redshift SNe Ia is performed using the spectral indicators described in section 2. The mean trends in the pseudo-EWs of the ‘Fe II 4800’ and ‘Mg II 4300’ features identified for normal – low-redshift – SNe Ia can be used to test whether or not high-redshift supernovae pseudo-EWs follow the same trends.

Table 11 Measurements of the pseudo-EWs of Ca II H&K, Mg II and Fe II. Measurements uncertainties are reported in parenthesis.^a

SN	epoch [days]	Ca II H&K pseudo-EW [Å]	Mg II pseudo-EW [Å]	Fe II pseudo-EW [Å]
sn2001gy	-7.5 (1)	176 (8/21)	111 (12/31)	
sn2002fd	-7 (2)	73.6 (3/14)	101 (8/11)	86 (15/23)
sn2000fr	-5.5 (1)	122 (13/14)	103 (6/13)	91 (13/23)
sn2001gw	-1 (2)	130 (9/13)	125 (17/22)	
sn2002gl	0 (2)	124 (14/15)	121 (12/18)	168 (20/25)
sn2001ha	0 (2)	188 (19/22)	132 (9/24)	216 (33/62)
sn2001hc	0 (2)	112 (15/15)	116 (11/18)	140 (15/23)
sn2001gr	2 (2)	94.6 (10/22)	140 (16/34)	141 (31/69)
sn2001gm	5 (2)	128 (23/26)	123 (17/40)	169 (34/84)
sn2001go	5.6 (1)	120 (11/28)	93 (11/24)	191 (28/41)
sn2002gk	6 (2)	91 (6/11)	161 (14/16)	157 (16/17)
sn2001go	9.5 (1)	112 (6/13)	181 (14/24)	174 (20/27)
sn2001go	29.5 (1)	228 (22/48)	315 (41/52)	

^aThe first value includes statistical and systematic uncertainties related to the level of host galaxy contamination, the second value (added in quadrature) also includes possible systematic uncertainties due to misidentification of the fitting regions, (see sec. 2 for details).

The results of a set of χ^2 tests are shown in Table 12. The intrinsic dispersion around the fitted mean trends for normal low- z supernovae was added in quadrature to the statistical and systematic uncertainties to perform the test. The uncertainty in the SN Ia phase was propagated according to the pseudo-EW model for normal low redshift SNe Ia and added in quadrature to the measurements error on the pseudo-EWs. The possible systematic uncertainties due to misidentification of the maxima was included was also taken into consideration. We note that the fitting region uncertainties — included in the results shown in Table 12 — should be considered as upper limits to the possible systematic uncertainty due to the pseudo-EW’s measurement technique (see section 2 for details).

The hypothesis that the pseudo-EW measured on our high-redshift supernovae follow the same behavior with lightcurve phase as those measured on low redshift normal supernovae is statistically confirmed. Moreover, the hypothesis that pseudo-EWs measured on our high-redshift supernovae are consistent with those of under-luminous SN 1991bg-like low redshift SNe Ia is rejected.

5. Summary and Conclusions

Spectroscopic data of 12 high-redshift supernovae, in the redshift interval $z=0.212$ to 0.912 , were analyzed and a qualitative classification scheme was presented. Based on this classification scheme, all of our high-redshift SNe Ia were classified as normal SNe Ia, except for SN 2002fd ($z=0.27$), which is similar to SN 1999aa, a peculiar 91T-like SN Ia. We also find, based on spectral properties alone, that none of the supernovae studied in this work are under-luminous. This is not unexpected because of the bias against selecting such objects in magnitude limited surveys (see for example Li et al. (2001a)).

A quantitative comparison between low and high-redshift SNe Ia by means of spectral indicators has been presented. The velocities of the minimum of Ca II H&K feature of high-redshift SNe Ia, were compared to those of low-redshift SNe Ia with the aim of uncovering differences. No systematic differences could be found.

Using a low-redshift SN Ia sample, we study the evolution in the pseudo-EW of the strongest spectral features as a function of phase, and find that the pseudo-EW of different SNe Ia sub-types (normal, 91T-like and 91bg-like) evolve differently for two of the three features studied (i.e. “Fe II 4800” and “Mg II 4300”). In the case of “Fe II 4800”, the different SNe Ia sub-types follow similar trends, but offset from the average evolution. 91bg-like SNe Ia show higher pseudo-EWs and 91T-like SNe Ia lower pseudo-EWs than normal SNe Ia. The pseudo-EW of “Mg II 4300” is characterized by a sudden break around maximum light. The epoch at which the break occurs correlates with the photometric properties of the SNe Ia. We find that in 91bg-like SNe Ia the break occurs earlier in phase with respect to normal SNe Ia while in 91T-like SNe Ia the same occurs later.

The pseudo-equivalent widths of “Fe II 4800”, “Mg II 4300” and “Ca II H&K” in high-redshift SNe Ia are found to follow the same trends with epoch as those observed in normal low-redshift SNe Ia. Furthermore, the pseudo-equivalent widths of “Fe II 4800” and “Mg II 4300” in high-redshift SNe Ia are found to be statistically consistent with the pseudo-equivalent widths observed in low-redshift normal SNe Ia.

The pseudo-EWs of Ca II H&K in the spectrum of SN 2002fd are consistent with those observed in SN 1991T/SN1999aa-like objects in the local Universe, quantitatively confirming the sub-type identification of

Table 12 A statistical comparison of the ‘Fe II 4800’ and ‘Mg II 4300’ pseudo-equivalent widths of high and low-redshift SNe Ia.

Feature	χ^2_{norm} (2)	P_{norm} (3)	$\chi^2_{91\text{bg-like}}$ (4)	$P_{91\text{bg-like}}$ (5)	χ^2_{norm} (6)	P_{norm} (7)	$\chi^2_{91\text{bg-like}}$ (8)	$P_{91\text{bg-like}}$ (9)
Fe II	13.0(11)	0.29	29.6(11)	0.002	6.7(11)	0.8	16.8(11)	0.1
Mg II	11.2(13)	0.59	228.4(13)	0.00	7.3(13)	0.9	162.4(13)	0.00

Columns 2, 3, 6 and 7 report the χ^2 correspond to the comparison of the pseudo-EWs ‘Fe II 4800’ and ‘Mg II 4300’ of high redshift SNe Ia with the fits for normal supernovae. Columns 4, 5, 8 and 9 report the comparison with under-luminous SNe Ia (e.g. SN 1986G and SN 1991bg). Columns 2, 4, 6, and 8 reports the χ^2 obtained with the number of degrees of freedom in parenthesis. Columns 3, 5, 7, and 9 report the probability to obtain a χ^2 value greater than that obtained. Columns 2 to 6 report the results including both statistical uncertainties and systematic uncertainties due to host galaxy subtraction. Columns 7 to 9 report the results when the systematic uncertainty due to possible misidentification of fitting regions is also included.

this SN Ia. This feature can be used to identify 91T-like objects at high-redshift.

The number of higher-redshift supernova used in this case study is small when compared to the numbers of SNe Ia that are now being observed at similar redshifts. Both the ESSENCE and SNLS projects will result in samples of SNe Ia with similar spectral quality; however, the samples will be many times larger. The case study presented here offers a simple method to analyze the spectra observed in these surveys and look for systematic differences between SNe Ia at different redshift.

References

- Astier, P., Guy, J., Regnault, N., et al. 2006, *A&A*, 447, 31
- Balland, C., Mouchet, M., Pain, R., et al. 2006, *A&A*, 445, 387
- Barris, B. J., Tonry, J. L., Blondin, S., et al. 2004, *ApJ*, 602, 571
- Blakeslee, J. P., Tsvetanov, Z. I., Riess, A. G., et al. 2003, *ApJ*, 589, 693
- Blondin, S., Dessart, L., Leibundgut, B., et al. 2006, *AJ*, 131, 1648
- Branch, D., Dang, L. C., Hall, N., et al. 2006, *PASP*, 118, 560
- Branch, D., Lacy, C. H., McCall, M. L., et al. 1983, *ApJ*, 270, 123
- Cardelli, J. A., Clayton, G. C., & Mathis, J. S. 1989, *ApJ*, 345, 245
- Coil, A. L., Matheson, T., Filippenko, A. V., et al. 2000, *ApJ*, 544, L111
- Cristiani, S., Cappellaro, E., Turatto, M., et al. 1992, *A&A*, 259, 63
- Filippenko, A. V. 1997, *ARA&A*, 35, 309
- Filippenko, A. V., Richmond, M. W., Branch, D., et al. 1992a, *AJ*, 104, 1543
- Filippenko, A. V., Richmond, M. W., Matheson, T., et al. 1992b, *ApJ*, 384, L15
- Folatelli, G. 2004, Ph.D. Thesis, available at <http://www.cops.physto.se/>
- Gal-Yam, A., Maoz, D., Strolger, L. G., et al. 1999, in *International Astronomical Union Circular*, 1–+
- Garavini, G., Aldering, G., Amadon, A., et al. 2005, *AJ*, 130, 2278
- Garavini, G., Folatelli, G., Goobar, A., et al. 2004, *AJ*, 128, 387
- Garnavich, P. M., Bonanos, A. Z., Krisciunas, K., et al. 2004, *ApJ*, 613, 1120
- Garnavich, P. M., Kirshner, R. P., Challis, P., et al. 1998, *ApJ*, 493, L53+
- Gerardy, C. L., Höflich, P., Fesen, R. A., et al. 2004, *ApJ*, 607, 391
- Goldhaber, G., Groom, D. E., Kim, A., et al. 2001, *ApJ*, 558, 359
- Gray, D. F. 1992, *Science*, 257, 1978
- Hamuy, M., Maza, J., Pinto, P. A., et al. 2002, *AJ*, 124, 417
- Hardin, D., Afonso, C., Alard, C., et al. 2000, *A&A*, 362, 419
- Hoeflich, P., Wheeler, J. C., & Thielemann, F. K. 1998, *ApJ*, 495, 617
- Hook, I. M., Howell, D. A., Aldering, G., et al. 2005, *AJ*, 130, 2788
- Howell, D. A., Sullivan, M., Perrett, K., et al. 2005, *ApJ*, 634, 1190
- Jeffery, D. J., Leibundgut, B., Kirshner, R. P., et al. 1992, *ApJ*, 397, 304
- Kirshner, R. P., Jeffery, D. J., Leibundgut, B., et al. 1993, *ApJ*, 415, 589
- Knop, R. A., Aldering, G., Amanullah, R., et al. 2003, *ApJ*, 598, 102
- Krisciunas, K., Garnavich, P. M., Challis, P., et al. 2005, *AJ*, 130, 2453
- Leibundgut, B., Kirshner, R. P., Filippenko, A. V., et al. 1991, *ApJ*, 371, L23
- Leibundgut, B., Kirshner, R. P., Phillips, M. M., et al. 1993, *AJ*, 105, 301
- Lentz, E. J., Baron, E., Branch, D., Hauschildt, P. H., & Nugent, P. E. 2000, *ApJ*, 530, 966
- Li, W., Filippenko, A. V., Chornock, R., et al. 2003, *PASP*, 115, 453
- Li, W., Filippenko, A. V., & Riess, A. G. 2001a, *ApJ*, 546,

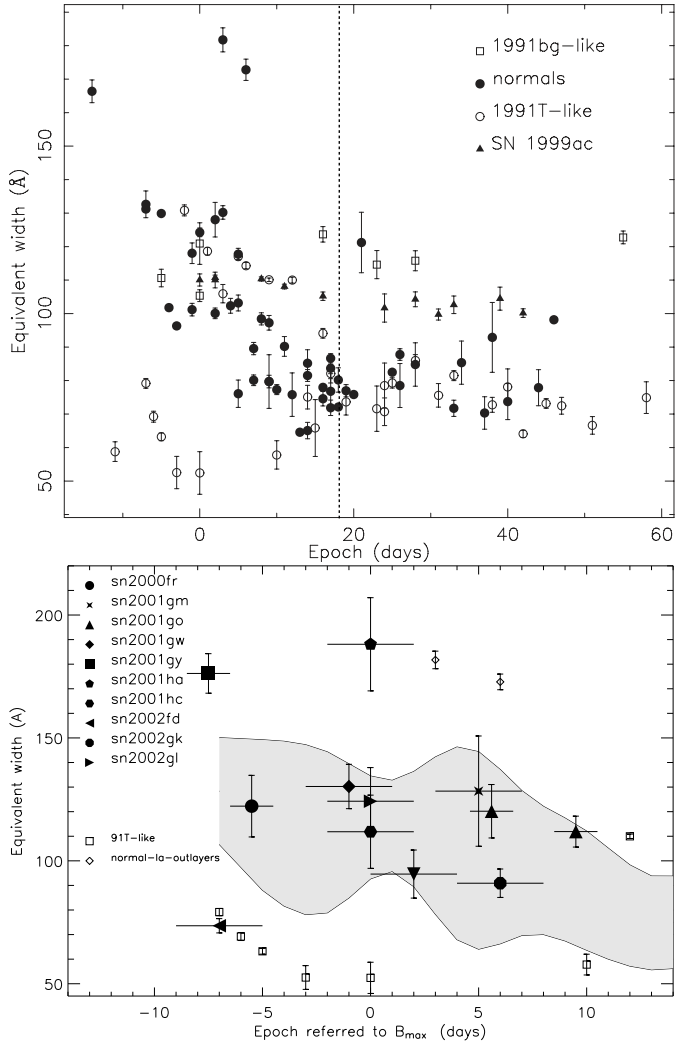


Fig. 8

“Ca II H&K”

Upper Panel: Measured pseudo-equivalent widths corresponding to “Ca II H&K” (#1). SN 1991bg-like objects are marked with open squares, 1991T-like SNe Ia with open circles, normal SNe Ia with filled circles and SN 1999ac with triangles. Error-bars include the error described by Eqn. 2 as well as systematic uncertainties arising from the pseudo-continuum fit. The vertical dashed line indicates the upper epoch limit in the lower panel. *Lower Panel:* A comparison between the ‘Ca II H&K’ pseudo-EWs in low and high-redshift SNe Ia. High-redshift supernova are indicated by large filled symbols. The gray filled area represents the 95% probability region for normal (non-outliers) and the under-luminous low-redshift SNe Ia SN 1999by, SN 1991bg and SN 1986G. Outliers normal SNe Ia are indicated with the diamond symbols. Slow declining SNe Ia are indicated by the open square symbols.

719

Li, W., Filippenko, A. V., Treffers, R. R., et al. 2001b, ApJ, 546, 734
 Lidman, C., Howell, D. A., Folatelli, G., et al. 2005, A&A, 430, 843
 Matheson, T., Blondin, S., Foley, R. J., et al. 2005, AJ,

129, 2352

Mazzali, P. A., Benetti, S., Altavilla, G., et al. 2005, ApJ, 623, L37
 Mazzali, P. A., Chugai, N., Turatto, M., et al. 1997, MNRAS, 284, 151
 Mazzali, P. A., Lucy, L. B., Danziger, I. J., et al. 1993, A&A, 269, 423
 Meikle, W. P. S., Cumming, R. J., Geballe, T. R., et al. 1996, MNRAS, 281, 263
 Patat, F., Benetti, S., Cappellaro, E., et al. 1996, MNRAS, 278, 111
 Perlmutter, S., Aldering, G., della Valle, M., et al. 1998, Nature, 391, 51
 Perlmutter, S., Aldering, G., Goldhaber, G., et al. 1999, ApJ, 517, 565
 Phillips, M. M., Krisciunas, K., Suntzeff, N. B., et al. 2002, From Twilight to Highlight - The Physics of Supernovae, ESO/MPA/MPE Workshop, Garching
 Phillips, M. M., Phillips, A. C., Heathcote, S. R., et al. 1987, PASP, 99, 592
 Phillips, M. M., Wells, L. A., Suntzeff, N. B., et al. 1992, AJ, 103, 1632
 Riess, A. G., Filippenko, A. V., Challis, P., et al. 1998, AJ, 116, 1009
 Riess, A. G., Strolger, L., Tonry, J., et al. 2003, astro-ph/0308185
 Riess, A. G., Strolger, L.-G., Tonry, J., et al. 2004, ApJ, 607, 665
 Ruiz-Lapuente, P., Cappellaro, E., Turatto, M., et al. 1992, ApJ, 387, L33
 Schaefer, B. E., Snyder, J. A., Hernandez, J., et al. 1999, ApJ, 524, L103
 Schlegel, D. J., Finkbeiner, D. P., & Davis, M. 1998, ApJ, 500, 525
 Schmidt, B. P., Suntzeff, N. B., Phillips, M. M., et al. 1998, ApJ, 507, 46
 Strolger, L.-G., Smith, R. C., Suntzeff, N. B., et al. 2002, AJ, 124, 2905
 Tonry, J. L., Schmidt, B. P., Barris, B., et al. 2003, ApJ, 594, 1
 Vinkó, J., Kiss, L. L., Csák, B., et al. 2001, AJ, 121, 3127
 Wells, L. A., Phillips, M. M., Suntzeff, N. B., et al. 1994, AJ, 108, 2233
 Wood-Vasey, W. M., Miknaitis, G., Stubbs, C. W., et al. 2007, ArXiv Astrophysics e-prints